J. Fluid Mech. (1996), *vol.* 323, *pp.* 387–409

Secondary instability of flow in a curved duct of square cross-section

By PHILIP A. J. MEES, K. NANDAKUMAR AND J.H. MASLIYAH

Department of Chemical Engineering, University of Alberta, Edmonton, Alberta, Canada T6G 2G6

(Received 19 May 1995 and in revised form 5 February 1996)

Experiments and simulations of a travelling wave state of incompressible Newtonian flow in a curved duct of square cross-section are presented. The travelling wave mode develops from the well-documented steady four-cell flow state and is characterized by oscillations of the two Dean vortices near the centre of the outer wall.

The oscillations were induced by a carefully positioned pin at 5° from the inlet of the curved section along the symmetry line of the cross-section. It was shown that the travelling wave state is characteristic for curved duct flow and that the pin made it possible to observe the oscillations within the 270° long curved duct. Travelling waves were observed at flow rates above $Dn = 170$ ($Dn = Re/(R/a)^{1/2}$, where Re is the Reynolds number, R is the radius of curvature of the duct and a is the duct dimension. The curvature ratio, R/a, is 15.1).

If no other disturbances are imposed, the oscillations are the result of the selective amplification of random disturbances in the flow, leading to a broad frequency spectrum. The travelling wave was found to lock in to an imposed periodic disturbance at a selected frequency. The flow structure of the locked state was investigated in detail, using flow visualization and a one-component laser Doppler anemometer to measure streamwise or spanwise velocities. Direct numerical simulations using the package CFDS-FLOW3D are in very good agreement with the experiments and confirm the existence of a fully developed, streamwise-periodic travelling wave state.

The inflow region between the two Dean vortices, which transports low-speed fluid away from the outer wall, creates strongly inflectional spanwise profiles of the streamwise velocity. Similarities with twisting vortices in a curved channel and sinuous oscillations of Görtler vortices show that the travelling waves observed here result from a secondary shear instability of these spanwise inflectional profiles.

1. Introduction

Since the early work by Dean (1927, 1928), most studies of flow in curved pipes and ducts have been concerned with steady flow phenomena. Review articles are available by Berger, Talbot & Yao (1983), Nandakumar & Masliyah (1986) and Itō (1987).

The solution structure of steady fully developed or two-dimensional flows in a curved duct of square cross-section was determined numerically by Winters (1987) and confirmed experimentally by Bara, Nandakumar & Masliyah (1992). For a loosely coiled duct, the main branch of two-cell flows is connected to a four-cell

branch through two folds at $Dn = 131$ and $Dn = 113$. The two-cell state consists of two counter-rotating Ekman vortices that are the result of the pressure gradients along the top and bottom walls. As a result of the primary instability, that is of centrifugal nature, two small Dean vortices are formed near the centre of the outer wall, which gives rise to a four-cell flow state. This four-cell state is unstable with respect to asymmetric disturbances, but was observed by Bara *et al.* (1992) because asymmetric disturbances in their experiment were small.

Winters (1987) calculated an isolated branch of two-cell and four-cell flows above $Dn = 191$. The four-cell state is unstable, while parts of the two-cell branch are stable. Between Dean numbers of 131 and 191 no stable two-dimensional solutions exist. Sankar, Nandakumar & Masliyah (1988) predicted steady spatial oscillations between two-cell and four-cell flows at Dean numbers above 131. These spatial oscillations were recently confirmed experimentally by Mees, Nandakumar & Masliyah (1996*b*).

Taylor (1929) had observed non-turbulent oscillations of two-cell flow in a helical pipe using dye visualization. Sinuous oscillations near the inner wall of a helical pipe were also observed by Sreenivasan & Strykowski (1983) and Webster & Humphrey (1993), who suggest that these are the result of an instability of the secondary jet coming off the centre of the inner wall. Oscillations in curved ducts of square cross-section were observed by Tsuda & Ohba (1984), Ohba, Tsuda & Takagi (1986), Belaidi, Johnson & Humphrey (1992) and Arnal, Goering & Humphrey (1992). The oscillations described in this paper show no similarities with earlier observations of oscillations in curved ducts, but have much in common with twisting vortices in curved channel flow and sinuous oscillations of Görtler vortices along a concave wall.

Two kinds of oscillating vortices have been observed in curved channel flow: short wavelength twisting vortices and long-wavelength undulating vortices (Kelleher, Flentie & McKee 1980; Finlay, Keller & Ferziger 1987, 1988; Ligrani & Niver 1988; Bottaro, Matsson & Alfredsson 1991; Matsson & Alfredsson 1992, 1993; Bottaro 1993; Le Cunff & Bottaro 1993). Several authors have shown that twisting vortices are the result of a shear instability of inflectional spanwise profiles of the streamwise velocity (Finlay *et al.* 1988; Matsson & Alfredsson 1992, Le Cunff & Bottaro 1993).

Two oscillating modes have also been observed in Görtler flow: a sinuous mode (e.g. Bippes & Görtler 1972; Bippes 1972) and a varicose mode (e.g. Ito 1980, 1985; Aihara & Koyama 1981). The sinuous mode has been related to spanwise inflectional profiles of the streamwise velocity (Swearingen & Blackwelder 1981; Floryan 1991; Yu & Liu 1991; Liu & Domaradzki 1993).

2. Experimental system

The curved section of the apparatus, which was 270° long, had a 1.27 cm square cross-section, and a curvature ratio, $R_c = R/a$, of 15.1 (figure 1). The cross-section coordinates were non-dimensionalized as $x = x'/a$ and $z = z'/a$.

A detailed description of the experimental setup is given by Mees, Nandakumar & Masliyah (1996*a*). Added to this system was a forcing mechanism, consisting of a peristaltic pump without its casing. The three rollers of the pump periodically compressed the hose that leads the water to the stilling chamber. The travelling wave locks in to the small periodic disturbance that was created by the forcing. The distance over which the hose was compressed by each of the rollers was adjustable.

The experimental techniques used were flow visualization with laser fluorescent dye and a one-component laser Doppler anemometer to measure streamwise or spanwise

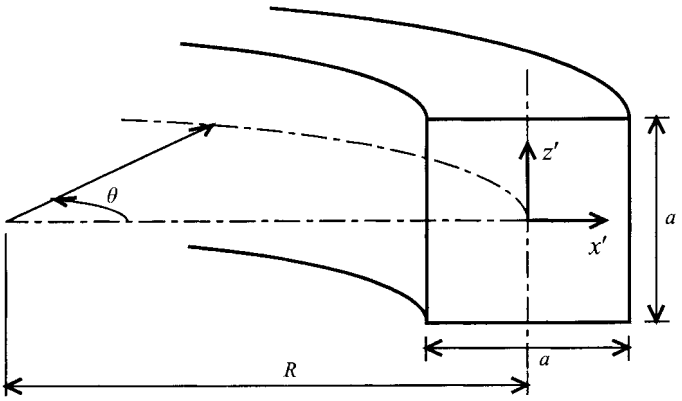

FIGURE 1. Curved duct geometry.

velocities. Secondary flow patterns were visualized using a laser light sheet. Streamwise flow patterns were made visible by illuminating a 10°–20° long section from above.

The flow conditions at the inlet of the curved section are described in detail by Mees (1994). According to the experimentally determined correlation by Goldstein & Kreid (1967), the flow in the 1 m long straight inlet section reaches a fully developed state up to a Dean number of 225. This was confirmed experimentally by Mees (1994). At higher flow rates, the inlet profiles are less and less developed, as is indicated by a growing flat region in the centre of the velocity profile.

3. Travelling wave experiments

The travelling wave state was induced by inserting a pin at 5° from the inlet of the curved section. The pin was inserted through the outer wall along the horizontal centreline, $z = 0$. Pin sizes of 33, 29, 27, 26 and 25 gauge were used with diameters of 0.2, 0.33, 0.41, 0.46 and 0.5 mm, respectively.

Side-view visualization of a typical travelling wave is shown in figure 2(*a*), at $Dn = 220$ ($Dn = Re/(R/a)^{1/2}$ where Re is the Reynolds number). The photographs were taken at different moments in time. In this case the time dependence starts around $\theta = 140°$. The oscillations of the flow are quite irregular. The travelling wave state seems to consist of a series of wave bursts, or packets, that grow and blend together as they travel downstream. One such a wave packet is visible in figure 2(*a*) between $\theta = 170°$ and $\theta = 175°$. The existence of these wave packets suggests that the flow is convectively unstable. The state of a convectively unstable system is determined by small disturbances that are selectively amplified in the direction of the flow.

In a moving reference frame, the dye pattern widens slowly while it is convected downstream. It is important to realize that the dye pattern in the photographs does not necessarily represent the secondary flow field. Because the dye moves at a different speed than the wave, the dye pattern will change with streamwise position, even if the flow field is fully developed or streamwise periodic.

The time series of cross-section visualizations in figure 3 shows that the two Dean vortices are oscillating while the large Ekman vortices remain relatively quiescent. A characteristic feature of the wavy flow is the oscillating inflow region between two Dean vortices, clearly visible in figure 3. The stagnation point near the centre of

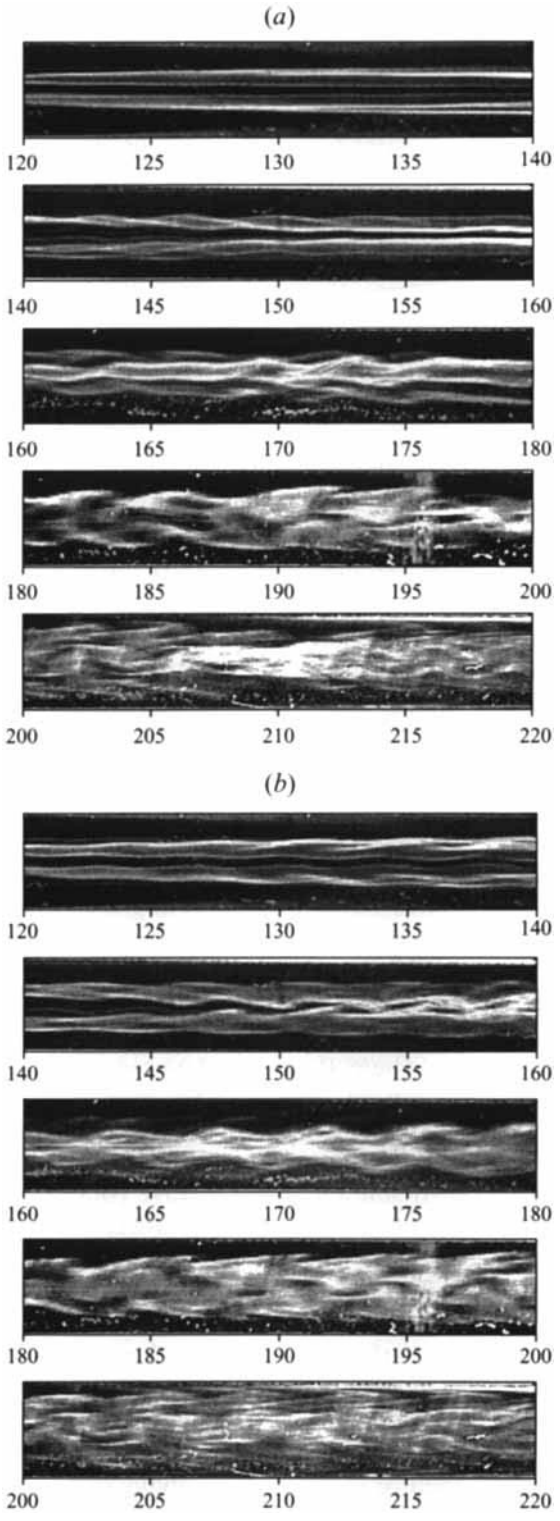

FIGURE 2. Side-view flow visualization of a developing travelling wave without forcing (*a*) and with forcing at 6.6 Hz (*b*). $Dn = 220$, 29 gauge pin. Dye was injected continuously.

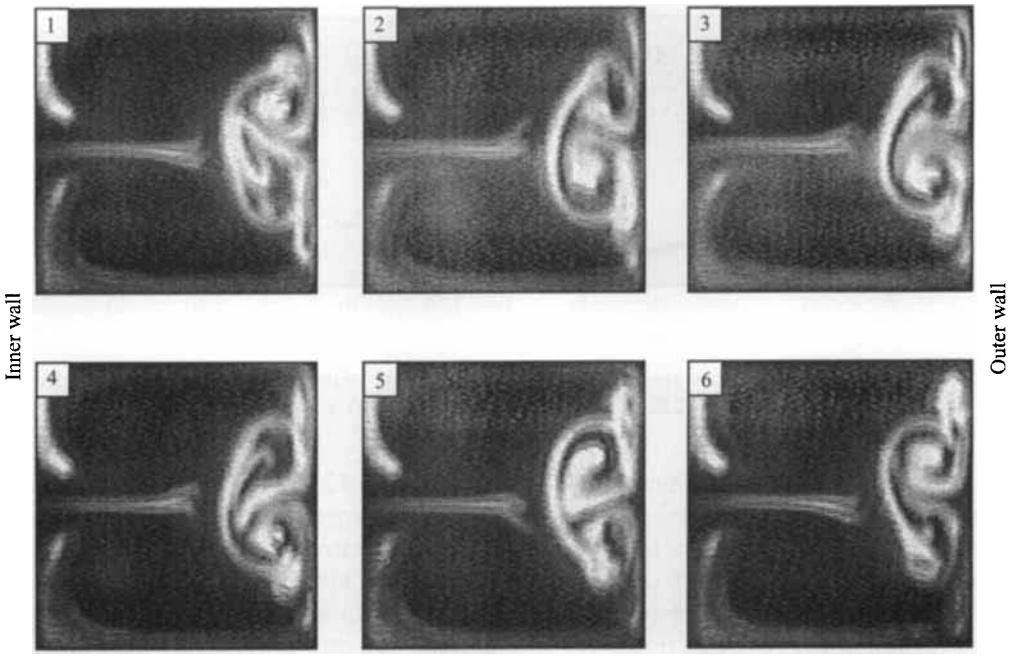

FIGURE 3. Cross-section flow visualization showing oscillations at $Dn = 220$ and $\theta = 200°$ with a 29 gauge pin.

the outer wall does not move. The centres of the Dean vortices seem to perform an almost circular motion with the upper Dean vortex rotating counterclockwise and the lower Dean vortex rotating in a clockwise direction.

The qualitative features discussed so far were quantified using detailed velocity measurements. Frequency analysis of the streamwise velocity fluctuations was used to determine which modes are present. Velocity fluctuations were measured at 61 positions along a spanwise line at $x = 0.27$ from $z = -0.24$ to $z = 0.24$ ($\pm$ 3 mm from the centreline). Strong velocity fluctuations are found in this region. All spectra of the unforced system show a broad maximum in the 5–8 Hz range, depending on the flow rate. The average frequency spectrum for a Dean number of 220 and $\theta = 180°$ is shown in figure figure 4(*a*). The broadband character of the frequency spectra confirms the convective instability of the flow.

One of the objectives of this study was to characterize the structure of the wavy flow. It is therefore necessary to study a single mode, rather than a combination of modes in a wide range of frequencies. Because the flow is very sensitive to upstream disturbances, a selected mode can be given an advantage over other modes by introducing a periodic disturbance that is larger than the disturbances created by random noise. This periodic disturbance was created by slightly compressing the Tygon hose that leads the water to the stilling chamber, using the rollers of a peristaltic pump. The velocity fluctuations that are caused by the forcing are two orders of magnitude smaller than the velocity fluctuations that are the result of the travelling wave. Depending on the forcing frequency and the forcing intensity, the excited mode can become the dominating mode, even if this is not the mode with the highest growth rate. Both in the unforced and the forced system the development of travelling waves is the result of small disturbances in the flow. There is no essential difference between the two, except for the nature of the disturbances.

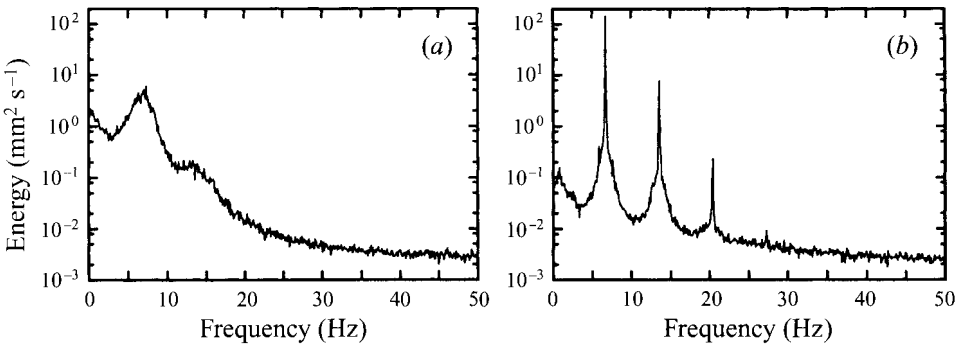

FIGURE 4. Averaged frequency spectra of streamwise velocity without forcing (*a*) and with forcing (*b*) at $Dn = 220$, $\theta = 180°$, $x = 0.27$ and with a 25 gauge pin.

The average frequency spectrum with forcing at 6.82 Hz but otherwise identical conditions as figure 4(*a*) is shown in figure 4(*b*). The energy of the mode corresponding to the forcing frequency is much higher than the energy of any other mode. The harmonics are the result of the structure of the flow and do not represent separate modes. The energy of other modes is much lower than in the unforced system. This suppression is the result of nonlinear interactions between different modes. The total wave power does not change significantly as a result of the forcing. The forcing merely causes a shift of energy from a wide range of modes to a single mode. A forcing frequency of 6.82 Hz is close to the fastest growing mode, however anywhere in the 3–10 Hz range the wave can lock in to the forcing frequency.

Side-view flow visualization of the forced system is shown in figure 2(*b*). The dye pattern is much more regular than in the unforced system and wave packets can be distinguished. Although the dye pattern changes continuously in the streamwise direction, over a small streamwise distance the pattern is shift-and-reflect symmetric. This means that the pattern is invariant over a reflection in the centreplane, combined with a spatial shift over half a streamwise wavelength.

The spatial development of the flow oscillations was quantified by measuring streamwise velocity fluctuation profiles at $x = 0.27$ and $-0.24 < z < 0.24$ for a series of streamwise positions. The total wave power and the power of the fundamental and first and second harmonic components (1.56 Hz wide bands) are plotted in figure 5. From $\theta = 80°$ to $\theta = 110°$, the wave power increases at a linear rate. Nonlinearities start to dominate the wave development around $\theta = 120°$, at which point the wave power begins to saturate. After $\theta = 170°$ the wave power does not change much with streamwise position. In this region the time-averaged flow field seems to be axially invariant, and this state will be called the 'fully developed wave' state.

4. Role of the pin in inducing time dependence

Flow visualization shows that the travelling wave state develops from a steady four-cell flow. Hence, in order to find a travelling wave state, both a steady four-cell flow state and disturbances that destabilize this four-cell state have to be present. The pin plays an important role in both these phenomena. Bara *et al.* (1992), who studied the development of steady flows up to $Dn = 150$, showed that the pin reduces the streamwise length needed to reach a fully developed steady four-cell state. By measuring how long it takes a sudden change in forcing frequency to reach the

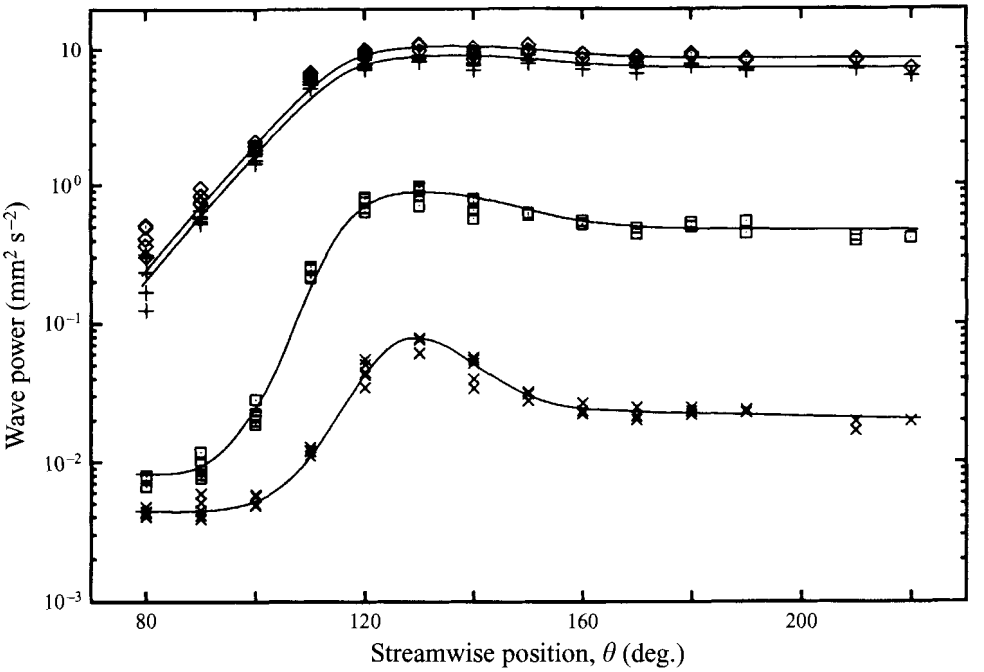

FIGURE 5. Spatial development of the streamwise velocity amplitude (◇, total amplitude; +, fundamental; □, first harmonic; ×, second harmonic). $Dn = 220$, $x = 0.27$, 25 gauge pin, average forcing frequency of 6.71 Hz. 61 samples ($-0.24 < z < 0.24$) of 512 measurements sampled at 100 Hz.

downstream position at $\theta = 180°$, it was determined that the disturbances that the wave locks in to are created by the pin.

Without inserting the pin no oscillations were observed within the first 270° for $170 < Dn < 260$ and one can only speculate about whether spontaneous oscillations would occur further downstream or not. Without the pin a four-cell state will develop, although somewhat further downstream (Bara *et al.* 1992). It seems likely that without the pin, random disturbances in the flow will grow and eventually destabilize the four-cell flow, although this may take much longer. This suggests that in a longer apparatus travelling waves would form spontaneously. Some experimental evidence exists for these spontaneous oscillations: without inserting the pin, oscillations develop near the end of the duct for Dn around 600. Highly unstable flow and very fast oscillations make what seem like naturally occurring travelling waves very difficult to study.

Vortex shedding was observed in the wakes behind all pins used in this study. In order to confirm that the travelling wave is a solution of curved duct flow, and not the result of wake oscillations, the onset and frequency of the wake oscillations and the travelling wave state were compared.

The flow rate at the onset of vortex shedding was determined for each of the five pin diameters. In each case the onset of vortex shedding took place at a flow rate above the onset of travelling waves. For example, onset of vortex shedding behind the 33 gauge pin took place at $Dn = 380$, while travelling waves were induced by this pin at a Dean number as low as 180.

Other experiments were conducted to compare the frequencies of the travelling wave and the vortex shedding. The shedding frequency for a 25 gauge pin at $Dn = 220$ was determined at 26.2 Hz, which is much higher than the wave frequency of 7 Hz at this

Direction	Min. (m)	Max. (m)	grid 1	grid 2	grid 3
spanwise	−0.00635	0.00635	32	46	58
radial	0.18561	0.19831	22	32	40
streamwise	0.0	0.012731	100	128	160

TABLE 1. Geometry and grid dimensions.

flow rate. Finally, the wave frequency at flow rates between $Dn = 170$ and $Dn = 260$ does not depend on the pin diameter, while the wake frequency depends strongly on the pin diameter (Schlichting 1979). These results show that the wave is not the result of wake oscillations.

5. Direct numerical simulations

Three-dimensional and time-dependent simulations of the fully developed travelling wave state at a Dean number of 220 were performed using the commercial CFD package CFDS-FLOW3D. First the simulation strategy will be discussed, followed by the geometry and the solution method. In the next section the simulation results will be compared to the experiments. The simulations will also be used to analyse the flow structure and the instability mechanism that causes the travelling waves.

Because of the very fine grid resolution that is required to resolve the travelling wave state, the streamwise extent of the computational domain had to be kept to a minimum. This was accomplished by imposing periodic boundary conditions in the streamwise direction. This streamwise periodicity creates a continuous feedback between the outlet and the inlet of the computational domain, which destroys the convective nature of the flow. Although this changes the dynamics of the system, the structure of the fully developed periodic flow, which is the objective of this simulation, is not affected.

Streamwise-periodic boundary conditions also change the stability of the steady four-cell flow state from which the travelling waves develop. Because steady four-cell flow is unstable with respect to asymmetric perturbations, asymmetries that are caused by round-off errors are amplified and eventually cause the flow to break down. This breakdown is an asymmetric process, during which the two Dean vortices move either up or down and fold up into one of the Ekman vortices. The travelling wave state can therefore only be modelled in a streamwise periodic simulation if asymmetric breakup is prevented, without making the development of travelling wave modes impossible. This was achieved by imposing shift-and-reflect symmetry. It will be shown in the next section that the fully developed travelling wave state is shift-and-reflect symmetric. Imposing shift-and-reflect symmetry does not therefore affect the travelling wave solution, but it does stabilize steady four-cell flow because the breakdown of steady four-cell flow is not shift-and-reflect symmetric.

The dimensions of the geometry are given in table 1. The spanwise and radial dimensions correspond to the dimensions of the experimental apparatus. The streamwise wavelength was fixed at 3.8°, which is close to the experimentally observed wavelength with forcing at 6.6 Hz (figure 2*b*). The wave frequency was allowed to develop naturally. Three different grids were used. The cells are uniformly distributed in the streamwise direction. In the spanwise and radial directions geometric compression was used to increase the grid resolution near the centre of the outer wall, where the flow oscillations are most prominent.

CFDS-FLOW3D solves the fully elliptic, three-dimensional, time dependent Navier-Stokes equation, using a control volume approach. Hybrid differencing was used to model the convective terms of the transport equations. Block Stone's method was used to solve the linearized difference equations for the velocity components in the inner iteration. The SIMPLEC algorithm (Patankar 1980; Van Doormal & Raithby 1984) was used for the pressure coupling of the outer iteration with under-relaxation factors for the velocity components of 0.8. The time-stepping procedure used Crank–Nicolson differencing. Each time step was considered to be converged when the residual mass flow over the entire domain was less than 10^{-6}. Simulations were carried out on IBM RS/6000 model 560 computers with 256 and 512 Mb.

The simulations were either started from a slightly perturbed steady four-cell solution, or from the fully developed wave state calculated with a coarser grid. Using the finest grid, a fully developed wave state was reached after 8 s of real time. This simulation took 235 Mb of RAM and the CPU time for one time step of 0.0025 s was about 65 minutes, resulting in a total simulation time of over four months.

The frequency of the travelling wave that was selected by the temporal simulation with grid 3 was 6.45 Hz, which is very close to the 6.6 Hz of the experiment that the fixed wavelength for the simulation was based on.

6. Flow structure

One of the main objectives of this study of travelling waves in a curved square duct was to characterize the structure of the wavy flow. Experimentally, this was done by measuring amplitude and phase distributions. Numerical simulations provide further insight into the flow structure, in particular the vorticity field. The experimental and numerical investigation focused on the fully developed travelling wave state at a Dean number of 220. All simulation results in this section were calculated with the finest grid.

6.1. *Amplitude and phase distributions*

A velocity signal can be represented in the frequency domain as a sum of cosine functions, each with their own amplitude and phase. Since velocity signals in the forced system contain only a few frequency components, the fluctuating velocity field can be described very efficiently by the amplitude and phase of these components. The streamwise velocity fluctuations are strongest near the inflow region, and fluctuation characteristics change much more quickly in the spanwise direction than in the radial direction. Therefore, velocity fluctuations were measured along a spanwise line at $x = 0.27$. Amplitude and phase distributions show how the amplitude and phase of a certain frequency component vary with the spanwise position along this line.

The phase of the velocity fluctuations is only meaningful if it is defined relative to a phase reference. Phase distributions calculated with the forcing pump as phase reference were fairly noisy. Internal phase referencing was also used, by calculating the phase difference between different frequency components of the same velocity signal. Internal phase referencing produced much more reproducible results.

Velocity fluctuations were measured at a Dean number of 220 and $\theta = 180°$. At this position and flow rate the travelling wave has reached a fully developed state (figure 5). Typical amplitude and phase distributions of the streamwise velocity are shown in figure 6. Measured amplitude distributions are usually slightly asymmetric as a result of small disturbances in the flow. No systematic asymmetries were observed. The amplitude of the fundamental frequency reaches zero in the centre of the duct,

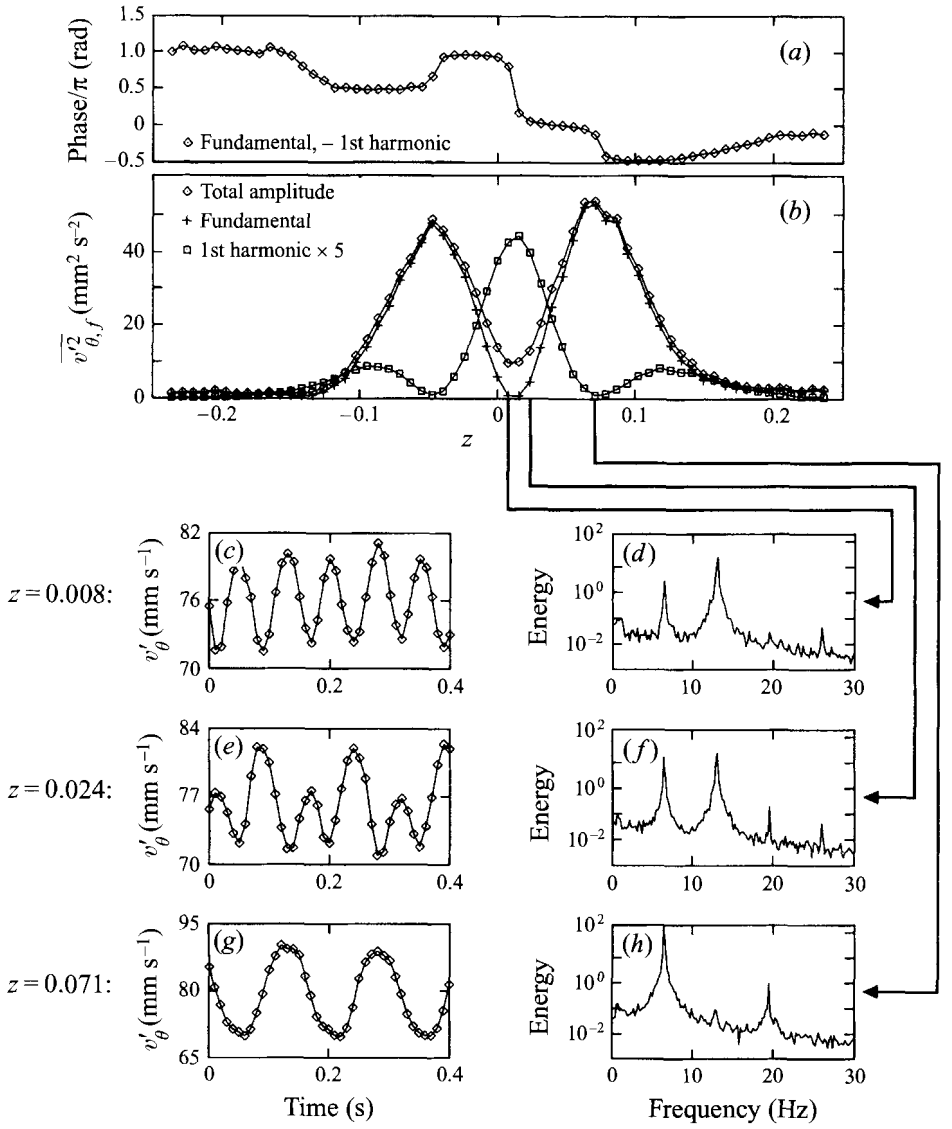

FIGURE 6. Streamwise velocity amplitude and phase distributions of fundamental and first harmonic (*a,b*). Time series and spectra illustrate the shift of power between the fundamental frequency and the first harmonic (*c–h*). $Dn = 220$, $\theta = 180°$, $x = 0.27$, 25 gauge pin, forcing at 6.5 Hz, 61 samples ($-0.24 < z < 0.24$) of 2048 measurements sampled at 100 Hz.

with maxima on both sides of the horizontal centreline. The first harmonic has a maximum in the centre and goes to zero around $z = \pm 0.05$ with secondary maxima around $z = \pm 0.1$.

The shift of power between the fundamental frequency and the first harmonic near the centre of the duct is illustrated in figure 6(*c–h*). At $z = 0.008$, close to the centreline and at the minimum of the fundamental amplitude, the first harmonic dominates the signal. At $z = 0.024$ the fundamental and the first harmonic are equally strong and at $z = 0.071$, where the fundamental frequency is at its maximum, the signal is dominated by the fundamental. The time series on the other side of the

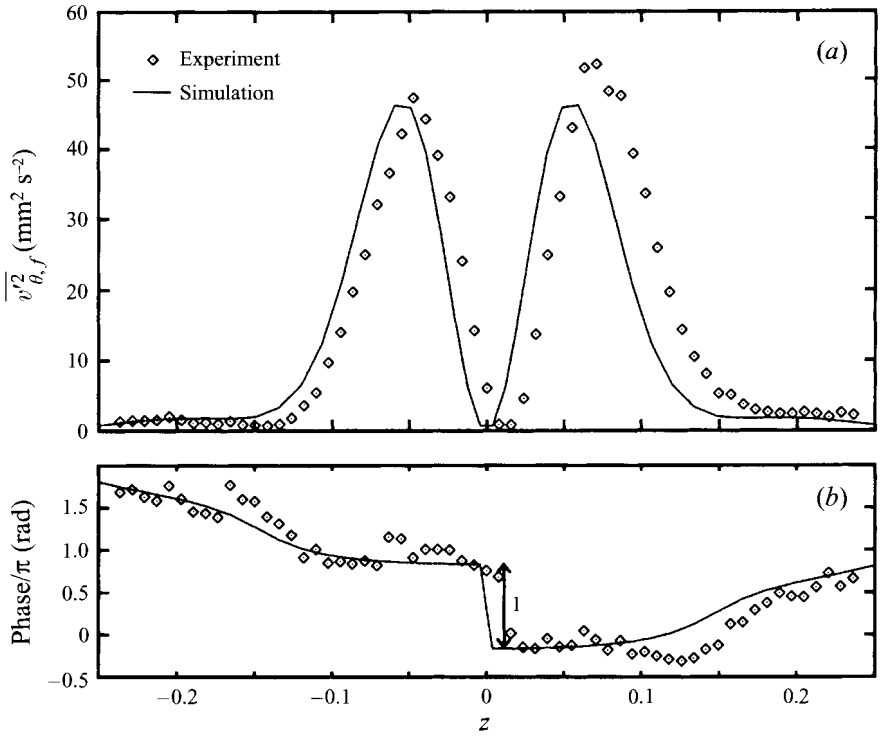

FIGURE 7. Streamwise velocity amplitude distribution (*a*) and phase distribution (*b*) of the fundamental component. Parameters as in figure 6.

centreline show the same trends. The phase jump at the centreline in figure 6(*a*) is associated with the fundamental frequency and will be explained in §6.2, where the symmetry of the flow is discussed.

Amplitude distributions of the streamwise velocity and distributions of the phase difference with the forcing signal are shown in figures 7 and 8 for the fundamental and first harmonic respectively. All phase differences are expressed as a fraction of the fundamental wavelength. Because of the arbitrary distance between the pin, where the forcing disturbances are created, and the position where the velocity is sampled, this phase difference is relative.

The phase differences with the forcing signal show a significant random fluctuation which makes it difficult to detect phase jumps. The uncertainty in the phase is probably caused by the relatively large distance between the pin and the position where the phase is measured, in this case at $\theta = 180°$. The forcing pump determines the phase of the disturbance that is created near the inlet of the duct. It takes the disturbance about 50 wavelengths, or 7 s, to travel to the position where the velocity is measured. Hence, the velocity and forcing signals at any point in time are not directly related. Because of the delay, small fluctuations in the forcing frequency or flow rate cause large uncertainties in the phase difference between the forcing signal and the velocity measured at $\theta = 180°$.

There is a π phase jump of the fundamental component in the centre of the duct. The first harmonic has two phase jumps of $\frac{1}{2}\pi$ each at about $z = \pm 0.05$. The solid lines in figures 7 and 8 are the results of the CFDS-FLOW3D simulation. The predicted phase distributions agree well with the experiments, especially with the uncertainty of

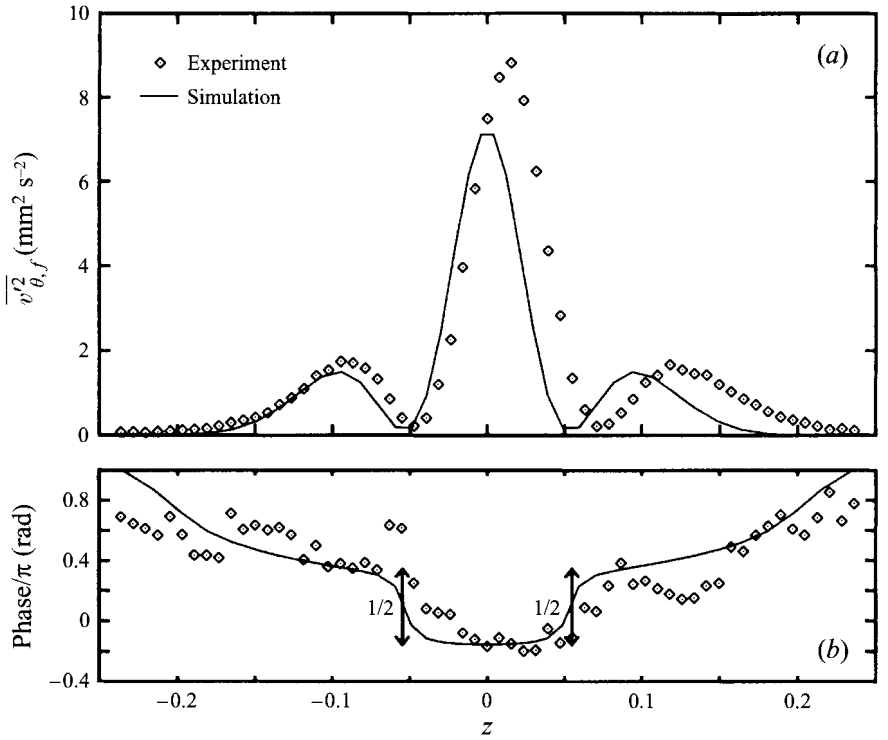

FIGURE 8. Streamwise velocity amplitude distribution (*a*) and phase distribution (*b*) of the first harmonic. Parameters as in figure 6.

	Experiment	grid 3	grid 2	grid 1
Total power	8.21	7.35	5.95	3.58
Fundamental	7.23	6.76	5.60	3.48
1st Harmonic	0.696	0.551	0.329	0.0971
2nd Harmonic	0.0387	0.0299	0.0127	0.00212

TABLE 2. Experimental and simulated wave power of the streamwise velocity (mm^2 s^{-2}).

the measured phase in mind. The amplitude distributions show the right trends, but are slightly lower than the experimental distributions. The experimental wave power of the streamwise velocity and the wave power predicted by the three simulations are given in table 2. Although the simulated wave power increases significantly with grid refinement, all simulations show qualitatively very similar oscillations of the Dean vortices. The amplitude of these oscillations increases with increasing grid resolution. It is likely that the amplitude will increase even more with further grid refinement, but this has not been done due to the large amount of computer memory and CPU time needed for such a simulation.

The phase differences between different frequency components of the velocity are much more reproducible than phase differences with the forcing signal. Shown in figure 9 is the phase difference between the fundamental and the first harmonic. The phase jumps are much more distinct than before. The simulated phase distribution

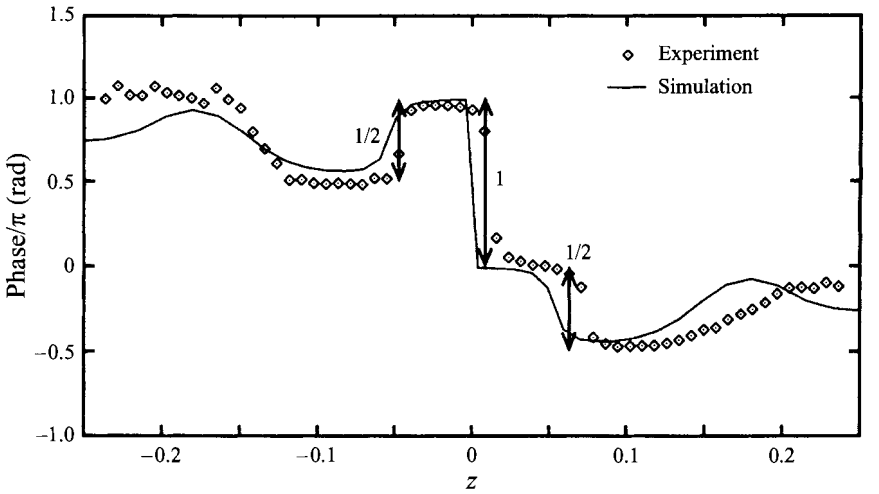

FIGURE 9. Phase difference between the fundamental and the first harmonic of the streamwise velocity. Parameters as in figure 6.

is in good agreement with the experiments. The phase differences with the second harmonic (not shown) are also in good agreement with the experiment.

Amplitude and phase distributions were also measured for the spanwise velocity. The amplitude of the fundamental component has a single maximum at the centreline, while the first harmonic is zero in the centre with maxima on either side. There are no phase jumps in the fundamental. The first harmonic has a $\frac{1}{2}\pi$ phase jump in the centre. All simulated amplitude and phase distributions show good qualitative agreement with the experiments.

6.2. *Symmetry*

The symmetries of a system are those transformations that leave that system apparently unchanged. The symmetries of the apparatus are considered first, because performing any of these symmetry transformations to a solution of the flow must lead to another valid solution, although not necessarily the same one.

Because the Dean problem is an open system with developing flow, it does not have rotational symmetry in the streamwise direction. However, an idealized system consisting of an infinitely long curved duct without entrance and exit regions does have rotational symmetry, just like Taylor–Couette flow. Another symmetry of the real and idealized apparatus is reflect symmetry around the centreplane, $z = 0$. Finally, because the apparatus does not change with time, it possesses all possible time symmetries.

The fully developed two-cell state, which is the primary solution for this geometry, has the same symmetries as the entire apparatus: no symmetry has been broken. The transition to a fully developed four-cell state does not break symmetry either. When travelling waves develop from steady four-cell flow, the time symmetry is broken by a Hopf bifurcation, leading to time-periodic solutions. At the same time the rotational symmetry is broken. A travelling wave is characterized by mixed spatio-temporal symmetry: the flow field is invariant over a rotation, combined with a translation in time by a corresponding amount, which is determined by the wave speed. Because this spatio-temporal symmetry makes space and time interchangeable, the spatial structure of the flow in this region can be determined by investigating the time-periodic flow

field at an arbitrary position in the fully developed wave region. The temporal flow structure was represented by the amplitude and phase distributions in the previous section.

Since the apparatus has reflect symmetry in the centreplane ($z = 0$), reflection of the travelling wave in the centreplane must produce either the same solution or a different, but also valid, solution. There are two different periodic travelling wave solutions that meet this requirement: the sinuous mode and the varicose mode. The varicose mode is symmetric in the centreplane, while the sinuous mode is shift-and-reflect symmetric. It is clear from the flow visualization in §3 that the flow field is not symmetric in the centreplane. The observed travelling wave state must therefore have shift-and-reflect symmetry. All measured amplitude and phase distributions confirm this shift-and-reflect symmetry.

Because space and time are interchangeable, a spatial shift is equivalent to a temporal shift of a corresponding amount. The symmetry conditions of the travelling wave state are therefore given by:

$$\left.\begin{aligned} v_r(r,\theta,z,t) &= v_r(r,\theta+\lambda/2,-z,t) = v_r(r,\theta,-z,t-T/2), \\ v_\theta(r,\theta,z,t) &= v_\theta(r,\theta+\lambda/2,-z,t) = v_\theta(r,\theta,-z,t-T/2), \\ v_z(r,\theta,z,t) &= -v_z(r,\theta+\lambda/2,-z,t) = -v_z(r,\theta,-z,t-T/2), \end{aligned}\right\} \tag{6.1}$$

where λ is the wavelength and T the period of the oscillations.

The fact that the amplitude of the fundamental at the centreline is zero follows directly from the shift-and-reflect symmetry: because the streamwise velocity at the centreline is unaffected by the reflection, the streamwise velocity profile in the centre is periodic over half a fundamental wavelength, and consequently has no fundamental component.

6.3. *Simulation results*

Because the simulation results are in very good agreement with the measured amplitude and phase distributions of both the streamwise and spanwise velocity, it is expected that other simulation results also give an accurate description of the actual flow field, even though the phenomena are probably under resolved. In this section we will present simulation results of quantities that cannot easily be measured experimentally, such as the vorticity. These results provide additional information on the structure of the flow field and will also be used for qualitative guidance as to the instability mechanism.

Cross-section arrow plots over half a wavelength of the oscillations are given in figure 10. Because of the travelling wave character of the flow, these plots can either be interpreted as the temporal evolution at a fixed position, or the spatial variation at a fixed moment in time. The oscillation of the inflow region between the Dean vortices, which was observed in the flow visualization (figure 3), is clearly visible in these arrow plots.

Contour plots of the streamwise vorticity are shown in figure 11. There are only four vortical structures in the flow: two Ekman vortices and two Dean vortices. The other streamwise vorticity is associated with shear layers along the walls. Close examination of the streamwise vorticity shows that the vortices perform an approximately circular motion during the oscillations, very similar to that observed in the flow visualization. This circular motion gives the Dean vortices an approximately helical shape. Although a direct comparison with the experiment is not possible,

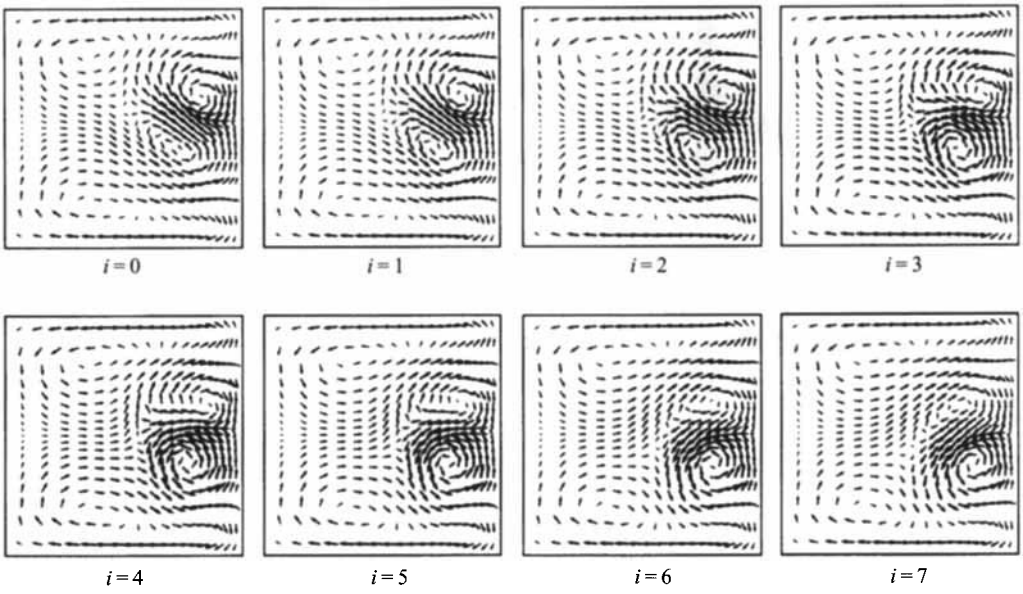

FIGURE 10. Arrow plots of the secondary velocity for $t = T(i/16)$ or $\theta = \lambda(1 - i/16)$. $Dn = 220$, $\lambda = 3.8°$.

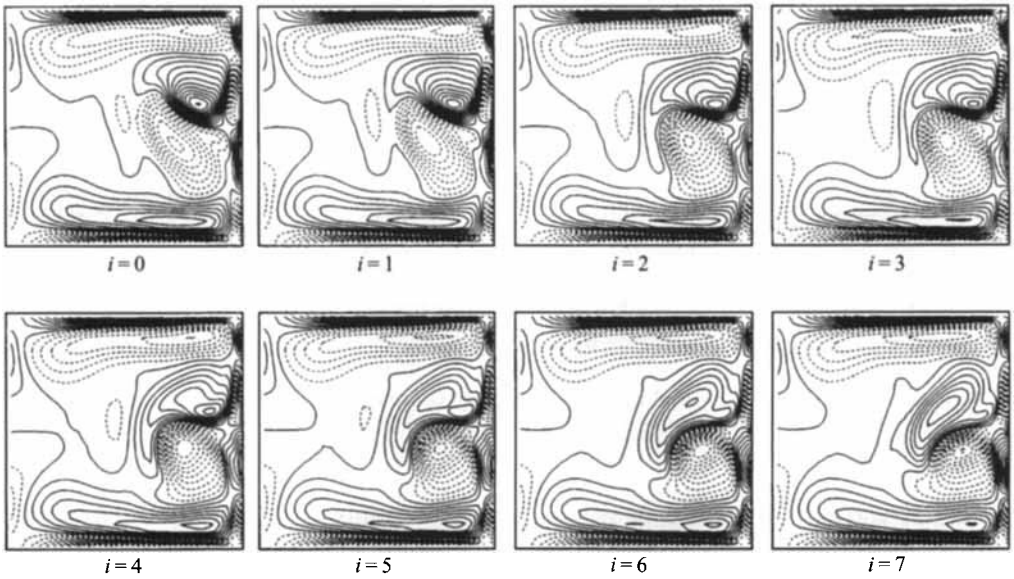

FIGURE 11. Streamwise vorticity plots in an (r,z)-plane for $t = T(i/16)$ or $\theta = \lambda(1 - i/16)$. $Dn = 220$, $\lambda = 3.8°$.

simulated streamwise vorticity and arrow plots show good qualitative agreement with the cross-section flow visualization of figure 3.

Contour plots of all velocity components in both the (r,z)- and the (θ,z)-planes are shown in figure 12. The streamwise velocity is more than an order of magnitude higher than the secondary velocities.

Contour plots of the radial vorticity in the (r,z)-plane and the radial vorticity and

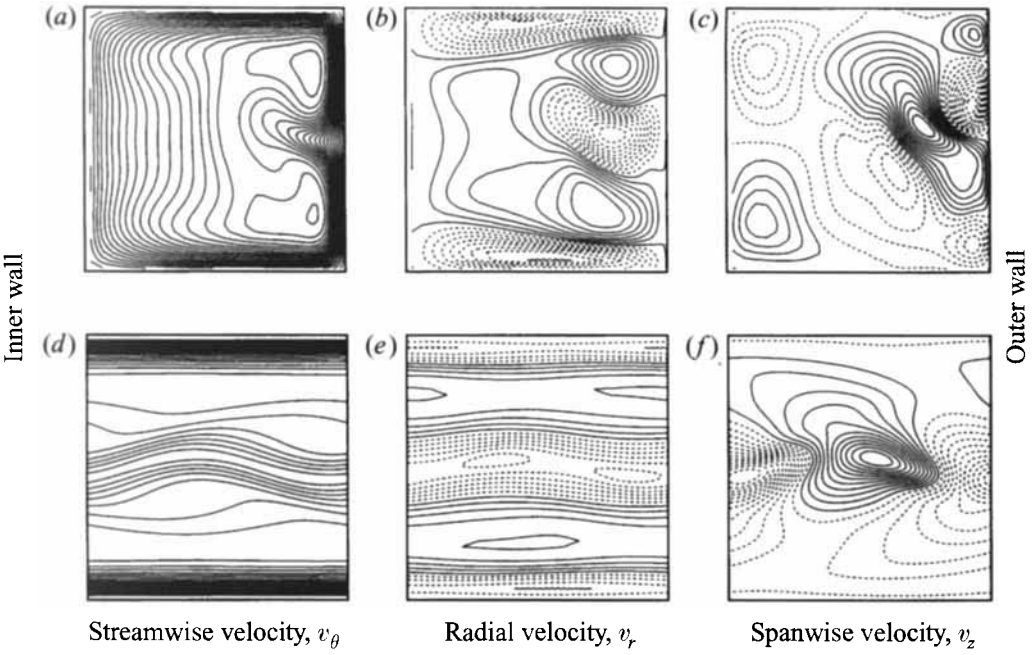

FIGURE 12. Velocity contour plots in the (r,z)-plane $(a$–$c)$ and (θ,z)-plane $(d$–$f)$. $Dn = 220$, $\lambda = 3.8°$. For $(d$–$f)$, $x = 0.27$.

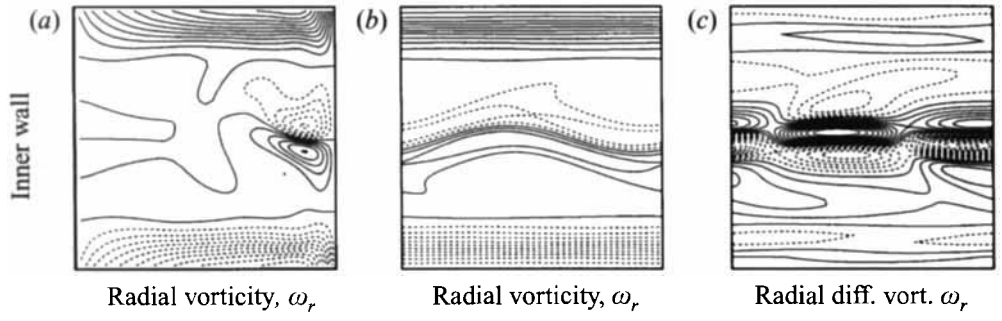

FIGURE 13. Radial vorticity and difference vorticity contour plots in the (r,z)-plane (a) and (θ,z)-plane (b, c). $Dn = 220$, $\lambda = 3.8°$, $x = 0.27$.

the radial vorticity difference in the (θ,z)-plane are shown in figure 13. Difference vorticity was defined as the vorticity field of the steady four-cell flow, subtracted from the vorticity field of the travelling wave state. There are regions with high radial vorticity on each side of the inflow region. This radial vorticity is associated with the spanwise inflectional profiles of the streamwise velocity. The radial vorticity near the top and the bottom walls is the result of the spanwise gradients of the streamwise velocity in those regions. The travelling wave state affects the radial vorticity much more strongly than the streamwise and spanwise vorticity fields.

A contour plot of the amplitude of the total streamwise velocity fluctuations is given in figure 14. There are two regions with high streamwise velocity oscillations, one on each side of the inflow region. Contours of the spanwise and radial gradients of the streamwise velocity of steady four-cell flow are also shown in figure 14. The regions

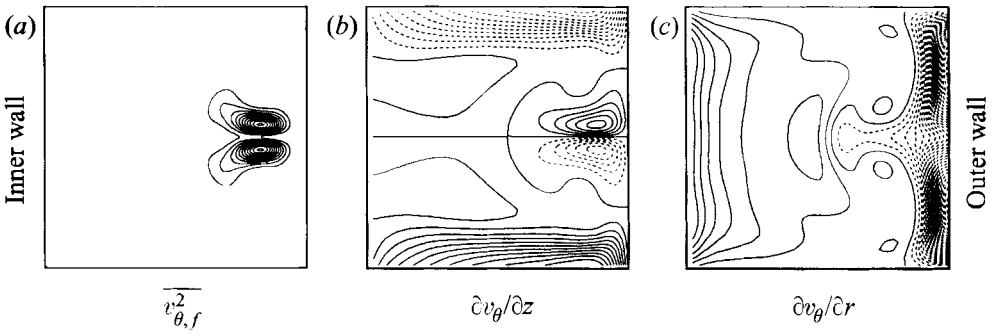

FIGURE 14. Amplitude of streamwise velocity fluctuations (*a*) and gradients of the streamwise velocity of steady two-dimensional four-cell flow (*b*,*c*) in an (*r*,*z*)-plane. $Dn = 220$, $\lambda = 3.8°$.

with high streamwise velocity fluctuations correspond to high spanwise gradients of the streamwise velocity.

This correlation between high spanwise gradients of the streamwise velocity and high streamwise velocity fluctuations is easily explained by examining how the spanwise velocity profile varies with time. The spanwise profile of the streamwise velocity at $x = 0.27$ during steady four-cell flow, simulated CFDS-FLOW3D, is shown in figure 15. The low velocity in the centre is due to the inflow region. Also shown are the spanwise profiles during the travelling wave state. The centre region with low streamwise velocity oscillates in the spanwise direction, while the shape of this centre region remains almost unchanged.

A simple model that explains the qualitative features of the measured amplitude and phase distributions is based on the assumption that the spanwise profile of the streamwise velocity does not change shape during the oscillations; the V-shaped centre region simply oscillates in the spanwise direction. The amplitude of the velocity fluctuations, induced by this oscillating profile, can then be determined from the shape of the spanwise velocity profile. Fluctuations at the fundamental frequency are, as a first approximation, proportional to the spanwise derivative of this profile and to the distance over which this profile oscillates in the spanwise direction (Δz). It can also be shown that the oscillations at the first harmonic frequency are, to a first approximation, proportional to the second derivative of the spanwise velocity profile, and to $(\Delta z)^2$.

The first two derivatives of the spanwise velocity profile of the streamwise velocity are shown in figure 16. The shapes of the derivatives agree remarkably well with the amplitude distributions from figure 6(*b*). The phase of the oscillations is related to the sign of the different derivatives. This simple model predicts phase jumps each time the amplitude is zero: in the centre for the fundamental and at $z = \pm 0.05$ for the first harmonic. This is in qualitative agreement with the phase distributions in figures 7(*b*) and 8(*b*).

Streamwise velocity fluctuations could also be the result of radial oscillations of the velocity profile, but the radial profile changes very little as a result of the travelling waves. Consequently, streamwise velocity fluctuations induced by radial oscillations are small compared to those induced by spanwise oscillations.

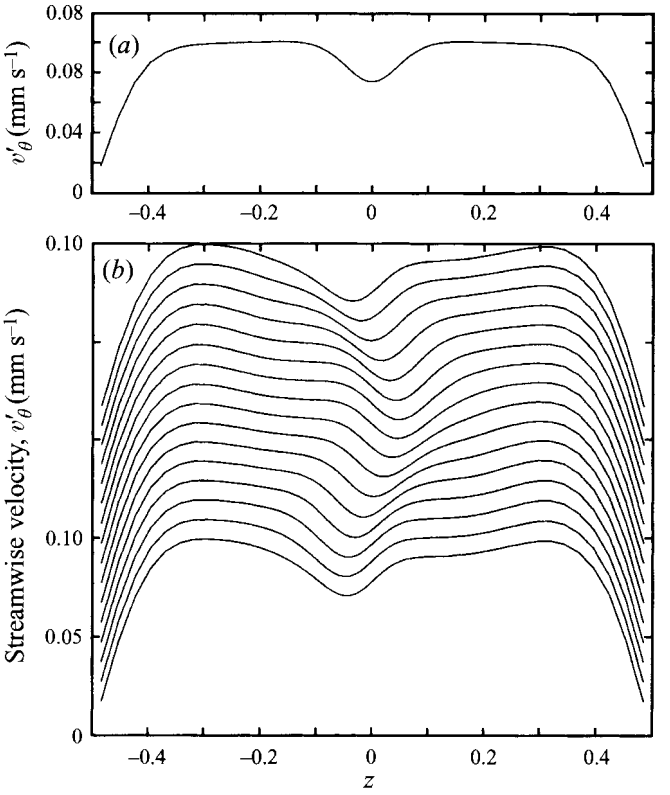

FIGURE 15. Simulated spanwise profiles of streamwise velocity in steady (*a*) and wavy (*b*) four-cell flow. $Dn = 220$, $\lambda = 3.8°$, $x = 0.27$.

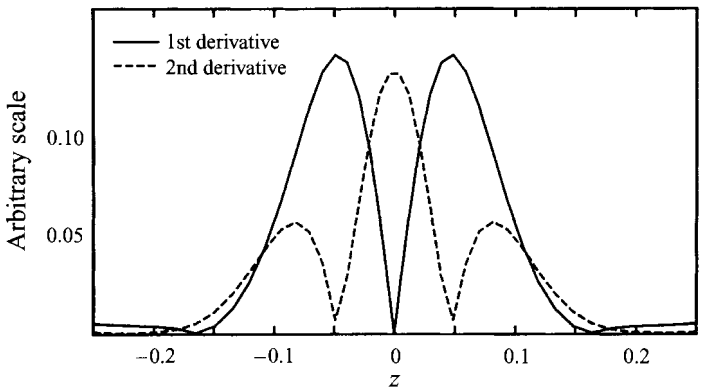

FIGURE 16. Derivatives of the spanwise profile of the streamwise velocity for steady four-cell flow. $Dn = 220$, $\lambda = 3.8°$, $x = 0.27$.

6.4. *Similarities with other systems*

6.4.1. *Curved geometries*

The travelling waves presented here show qualitative similarity with twisting waves in curved channel flow and the sinuous mode of wavy Görtler vortices. Twisting vortices in a curved channel were first observed experimentally by Kelleher *et al.* (1980)

and later simulated by Finlay *et al.* (1987, 1988). The arrow plots of secondary flow patterns of twisting waves in Finlay's *et al.* (1988) figure 16 are very similar to the ones in figure 10. In both cases the Dean vortices oscillate in the radial and spanwise directions and their strength fluctuates strongly. The inflow region oscillates in the spanwise direction, but the stagnation point near the outer wall does not move. Also, Finlay's plots of the radial and spanwise velocity in the (r,z)-plane (Finlay *et al.* 1987) are very similar to those in figures 12(*b*) and 12(*c*).

Two modes of wavy Görtler vortices have been observed: a varicose mode and a sinuous mode. The streamwise wavelengths of both modes are close to the spanwise wavelength. Swearingen & Blackwelder (1987) investigated experimentally the sinuous mode and found two regions with high streamwise oscillations, corresponding to high spanwise gradients of the streamwise velocity. The simulation results in figure 14 show a very similar correlation for wavy duct flow. Yu & Liu (1991) and Liu & Domaradzki (1993) found comparable results for simulated sinuous Görtler vortices. The simple model, which was used in §6.3 to explain the qualitative features of amplitude and phase distributions, forms a direct connection between high streamwise velocity fluctuations and high spanwise shear.

Swearingen & Blackwelder (1987) measured velocity fluctuations at different spanwise locations that show the same characteristics as the ones in figure 6(*c,e,g*). They also measured spanwise profiles of the streamwise velocity and observed a spanwise oscillation of the low-speed inflow region, very much like the simulated profiles in figure 15.

Liu & Domaradzki simulated the transition to turbulence in Görtler flow. Their contour plots of all three velocity components in a (θ,z)-plane of the sinuous mode of wavy Görtler vortices (before the transition to turbulence) are very similar to the contour plots in figure 12(*d–f*).

All available experimental and numerical work on wavy flows in curved channels and the Görtler problem suggests that the wavy Dean vortices in a curved square duct, twisting waves in a curved channel, and the sinuous mode of wavy Görtler vortices are different manifestations of the same phenomenon.

6.4.2. *Two-dimensional wakes*

This is the first study of wavy vortex flows in curved geometries that uses amplitude and phase distributions to characterize the structure of the flow. However, those distributions are commonly used to describe oscillating flow phenomena in two-dimensional wakes. It turns out that the amplitude and phase distributions of wavy curved duct flow are very similar to those of sinuous oscillations in a wake.

The first detailed experimental investigation of oscillations in the wake behind a flat plate was performed by Sato & Kuriki (1961), followed by many other experimental and numerical studies. Some studies focus on the structure of the oscillating flow, and the instability mechanism (Sato & Kuriki 1961; Mattingly & Criminale 1972), other studies focus more on mode interaction and the effect of forcing (Williams-Stuber & Gharib 1990; Williams, Mansy & Amato 1992).

Amplitude and phase distributions of both streamwise and spanwise velocity fluctuations have been used by many researchers to characterize the flow (Sato & Kuriki 1961; Sato 1970; Mattingly & Criminale 1972; Wygnanski, Champagne & Marasli 1986; Gharib & Williams-Stuber 1989; Marasli, Champage & Wygnanski 1989, 1992; Mansy & Williams 1991; Corke, Krull & Ghassemi 1992; Maekawa, Mansour & Buell 1992; Williams *et al.* 1992). The amplitude and phase distributions of the sinuous mode are generally very similar to the distributions presented here.

This similarity can easily be explained by considering the shape of spanwise profiles of the streamwise velocity. In both cases, these profiles have a V-shaped minimum near the plane of symmetry and the oscillating modes are characterized by a spanwise oscillation of this low-speed region, producing amplitude and phase distributions that are explained by our simple model. The radial vorticity field of the travelling wave state (figure 13) is very similar to the vorticity field of a developing vortex street (Abernathy & Kronauer 1962; Aref & Siggia 1981; Wygnanski *et al.* 1986).

7. Instability mechanism

A rigorous stability analysis of two-dimensional four-cell flow in a curved square duct to three-dimensional perturbations is not available in the existing literature, nor was it performed in the present study. However, stability analyses have been performed in other curved geometries, and also for two-dimensional wakes.

The instability mechanism for twisting waves in a curved channel was first studied by Finlay *et al.* (1988). They used an Orr–Sommerfeld analysis to calculate the stability of spanwise profiles of the streamwise velocity. Their results suggest that twisting waves are the result of a shear instability. The inflection points of the spanwise profiles play an important role in this shear instability.

A similar analysis was used by Le Cunff & Bottaro (1993) to study the stability of both spanwise and radial velocity profiles. They also found the twisting waves to be the result of a shear instability of spanwise inflectional profiles. The sinuous mode is always more unstable than the varicose mode.

Swearingen & Blackwelder (1987) found a strong correlation between the regions of high velocity fluctuations and high spanwise shear for the sinuous mode of oscillating Görtler vortices, and suggest that the oscillations are the result of an unstable velocity profile in the spanwise direction.

The V-shaped streamwise velocity profile of a two-dimensional wake is also unstable to a shear instability. It is this shear instability that causes the redistribution of the crosswise vorticity that leads to a von Kármán vortex street.

The inflectional spanwise velocity profiles in four-cell curved duct flow are very similar to those in curved channel flow, Görtler flow, and two-dimensional wakes. This similarity suggests that in a curved square duct also, the vortex oscillations are the result of a shear instability of spanwise inflectional profiles of the streamwise velocity. This instability mechanism indicates that the four-cell flow does not directly lead to travelling waves. Instead, the four-cell flow creates a streamwise velocity profile that is unstable to a secondary shear instability. It is this secondary instability that causes the transition to travelling waves. This qualitative information might be useful in any future three-dimensional stability analysis of curved duct flows.

8. Conclusions

Detailed experiments and numerical simulations of a fully developed travelling wave state in a curved duct of square cross-section were reported. This flow state has not been observed before. Experimentally the waves were observed at Dean numbers between 170 and 260, which is consistent with Winters' (1987) observation that no stable two-dimensional solutions exist above a Dean number of 131. In order to predict the onset of these travelling waves, a stability analysis of two-dimensional solutions to three-dimensional and time-dependent disturbances would have to be performed.

The experiments suggest that the travelling waves are the result of a convective instability of steady four-cell flow. In the experiments, the destabilizing disturbances were created by a pin that was inserted along the horizontal centreline, $z = 0$, at $\theta = 5°$, but it seems likely that in a longer duct the travelling wave state will develop spontaneously, induced by random disturbances. The convective nature of the flow was confirmed by the fact that the wave locks in to an imposed periodic disturbance.

Measured amplitude and phase distributions show that the flow has shift-and-reflect symmetry. These distributions, as well as the flow visualization, are in good agreement with streamwise-periodic simulations using CFDS-FLOW3D. As a result of the inflow region between the Dean vortices, the spanwise profiles of the streamwise velocity near the outer wall have a V-shaped minimum in the centre. During the travelling wave state, this V-shaped centre region oscillates in the spanwise direction, while its shape remains almost unchanged. A simple model that is based on the assumption that the spanwise profile does not change shape while oscillating explains all qualitative features of the amplitude and phase distributions.

The structure of the travelling waves in a curved square duct is very similar to that of twisting vortices in a curved channel and sinuous oscillations of Görtler vortices. Several authors have shown that twisting vortices are the result of a shear instability of spanwise inflectional velocity profiles. The waves also show similarities with a developing vortex street in a two-dimensional wake, which is the result of a shear instability. These similarities suggest that the travelling waves in a curved duct are also caused by a spanwise shear instability.

The financial support from the Natural Sciences and Engineering Research Council of Canada (NSERC) in the form of operating an equipment grants to K.N. and J.H.M. and from the University of Alberta in the form of a dissertation fellowship and the Andrew Stewart Memorial Graduate Prize to P.A.J.M. is gratefully acknowledged.

REFERENCES

ABERNATHY, F. H. & KRONAUER, R. E. 1962 The formation of vortex streets. *J. Fluid Mech.* **13**, 1–20.

AIHARA, Y. & KOYAMA, H. 1981 Secondary instability of Görtler vortices: Formation of periodic three-dimensional coherent structure. *Trans. Japan Soc. Aeronaut. Space Sci.* **24**(64), 78–94.

AREF, H. & SIGGIA, E. D. 1981 Evolution and breakdown of a vortex street in two dimensions. *J. Fluid Mech.* **109**, 435–463.

ARNAL, M. P., GOERING, D. J. & HUMPHREY, J. A. C. 1992 Unsteady laminar flow developing in a curved duct. *Intl J. Heat Fluid Flow* **13**, 347–357.

BARA, B., NANDAKUMAR, K. & MASLIYAH, J. H. 1992 An experimental and numerical study of the Dean problem: flow development towards two-dimensional multiple solutions. *J. Fluid Mech.* **244**, 339–376.

BELAIDI, A., JOHNSON, M. W. & HUMPHREY, J. A. C. 1992 Flow instability in a curved duct of rectangular cross-section. *Trans. ASME: J. Fluids Engng* **114**, 585–592.

BERGER, S. A., TALBOT, L. & YAO, L.-S. 1983 Flow in curved pipes. *Ann. Rev. Fluid Mech.* **15**, 461–512.

BIPPES, H. 1972 Experimentelle Untersuchung des laminar-turbulenten Umschlags an einer parallel angeströmten konkaven Wand. *Sitzungsber. Heidel. Akad. Wiss., Math.-naturwiss. Kl.* **3**, 103–180. Also *NASA Tech. Mem.* 75243 (1978).

BIPPES, H. & GÖRTLER, H. 1972 Dreidimensionale Störungen in der Grenzschicht an einer konkaven Wand. *Acta Mech.* **14**, 251–267.

BOTTARO, A. 1993 On longitudinal vortices in curved channel flow. *J. Fluid Mech.* **251**, 627–660.

BOTTARO, A., MATSSON, O. J. E. & ALFREDSSON, P. H. 1991 Numerical and experimental results for developing curved channel flow. *Phys. Fluids* A **3**, 1473–1476.

CORKE, T. C., KRULL, J. D. & GHASSEMI, M. 1992 Three-dimensional-mode resonance in far wakes. *J. Fluid Mech.* **239**, 99–132.

DEAN, W. R. 1927 Note on the motion of fluid in a curved pipe. *Phil. Mag.* **4**(7), 208–223.

DEAN, W. R. 1928 The stream-line motion of fluid in a curved pipe. *Phil. Mag.* **5**(7), 673–695.

FINLAY, W. H., KELLER, J. B. & FERZIGER, J. H. 1987 Instability and transition in curved channel flow. Rep. TF-30. Dept. of Mech. Engng, Stanford University, CA.

FINLAY, W. H., KELLER, J. B. & FERZIGER, J. H. 1988 Instability and transition in curved channel flow. *J. Fluid Mech.* **194**, 417–456.

FLORYAN, J. M. 1991 On the Görtler instability of boundary layers. *Prog. Aerospace Sci.* **28**, 235–271.

GHARIB, M. & WILLIAMS-STUBER, K. 1989 Experiments on the forces wake of an airfoil. *J. Fluid Mech.* **208**, 225–255.

GOLDSTEIN, R. J. & KREID, D. K. 1967 Measurement of laminar flow development in a square duct using a laser-Doppler flowmeter. *Trans. ASME: J. Appl. Mech.* **34**, 813–818.

ITO, A. 1980 The generation and breakdown of longitudinal vortices along a concave wall. *J. Japan Soc. Aeronaut. Space Sci.* **28**(318), 327–333.

ITO, A. 1985 Breakdown structure of longitudinal vortices along a concave wall. *J. Japan Soc. Aeronaut. Space Sci.* **33**(374), 166–173.

ITŌ, H. 1987 Flow in curved pipes. *JSME Intl J. II* **30**(262), 543–552.

KELLEHER, M. D., FLENTIE, D. L. & MCKEE, R. J. 1980 An experimental study of the secondary flow in a curved rectangular channel. *Trans. ASME: J. Fluids Engng* **102**, 92–96.

LE CUNFF, C. & BOTTARO, A. 1993 Linear stability of shear profiles and relation to the secondary instability of the Dean flow. *Phys. Fluids* A **5**, 2161–2171.

LIGRANI, P. M. & NIVER, R. D. 1988 Flow visualization of Dean vortices in a curved channel with 40 to 1 aspect ratio. *Phys. Fluids* **31**, 3605–3617.

LIU, W. & DOMARADZKI, J. A. 1993 Direct numerical simulation of transition to turbulence in Görtler flow. *J. Fluid Mech.* **246**, 267–299.

MAEKAWA, H., MANSOUR, N. N. & BUELL, J. C. 1992 Instability mode interactions in a spatially developing plane wake. *J. Fluid Mech.* **235**, 223–254.

MANSY, H. & WILLIAMS, D. R. 1991 Symmetry of interacting modes in a cylinder wake. *Phys. Fluids* A **3**, 2047–2049.

MARASLI, B., CHAMPAGNE, F. H. & WYGNANSKI, I. J. 1989 Modal decomposition of velocity signals in a plane, turbulent wake. *J. Fluid Mech.* **198**, 255–273.

MARASLI, B., CHAMPAGNE, F. H. & WYGNANSKI, I. 1992 Effect of traveling waves on the growth of a plane turbulent wake. *J. Fluid Mech.* **235**, 511–528.

MATSSON, O. J. E. & ALFREDSSON, P. H. 1992 Experiments on instabilities in curved channel flow. *Phys. Fluids* A **4**, 1666–1676.

MATSSON, O. J. E. & ALFREDSSON, P. H. 1993 Secondary instability and breakdown to turbulence in curved channel flow. *Appl. Sci. Res.* **51**, 9–14.

MATTINGLY, G. E. & CRIMINALE, W. O. 1972 The stability of an incompressible two-dimensional wake. *J. Fluid Mech.* **51**, 233–272.

MEES, P. A. J. 1994 Instability and transitions of flow in a curved duct of square cross section. PhD thesis, Department of Chemical Engineering, University of Alberta.

MEES, P. A. J., NANDAKUMAR, K. & MASLIYAH, J. H. 1996*a* Instability and transitions of flow in a curved square duct: the development of two pairs of Dean vortices. *J. Fluid Mech.* **314**, 227–246.

MEES, P. A. J., NANDAKUMAR, K. & MASLIYAH, J. H. 1996*b* Steady spatial oscillations in a curved duct of square cross-section. submitted to *Phys. Fluids.*

NANDAKUMAR, K. & MASLIYAH, J. H. 1986 Swirling flow and heat transfer in coiled and twisted pipes. *Advances in Transport Processes.* (ed. A. S. Mujumdar & R. A. Mashelkar), pp. 49–112. Wiley Eastern.

OHBA, K., TSUDA, N. & TAKAGI, K. 1986 A velocity fluctuation in developing laminar flow through a moderately curved U-bend of square cross-section. *Tech. Rep. Kansai Univ.* no. **27**, 33–42.

PATANKAR, S. V. 1980 *Numerical Heat Transfer and Fluid Flow.* Hemisphere.

SANKAR, S. R., NANDAKUMAR, K. & MASLIYAH, J. H. 1988 Oscillatory flows in coiled square ducts. *Phys. Fluids* **31**, 1348–1359.

SATO, H. 1970 An experimental study of non-linear interaction of velocity fluctuations in the transition region of a two-dimensional wake. *J. Fluid Mech.* **44**, 741–765.

SATO, H. & KURIKI, K. 1961 The mechanism of transition in the wake of a thin flat plate placed parallel to a uniform flow. *J. Fluid Mech.* **11**, 321–352.

SCHLICHTING, H. 1979 *Boundary-Layer Theory*, 7th edn. McGraw-Hill.

SREENIVASAN, K. R. & STRYKOWSKI, P. J. 1983 Stabilization effects in flow through helically coiled pipes. *Exps. Fluids* **1**, 31–36.

SWEARINGEN, J. D. & BLACKWELDER, R. F. 1987 The growth and breakdown of streamwise vortices in the presence of a wall. *J. Fluid Mech.* **182**, 255–290.

TAYLOR, G. I. 1929 The criterion for turbulence in curved pipes. *Proc. R. Soc. Lond.* A **124**, 243–249.

TSUDA, N. & OHBA, K. 1984 Laser Doppler measurement of developing laminar flow in a moderately curved U-bend of square cross-section. In *Laser Doppler Velocimetry and Hot Wire/Film Anemometry, Proc. Second Osaka Symp. on Flow Measuring-Techniques. July 13, Osaka, Japan.* pp. 1–15. Tokyo: The Power Company.

VAN DOORMAL, J. P. & RAITHBY, G. D. 1984 Enhancements of the SIMPLE method for predicting incompressible fluid flows. *Numer. Heat Transfer* **7**, 147–163.

WEBSTER, D. R. & HUMPHREY, J. A. C. 1993 Experimental observations of flow instability in a helical coil. *Trans. ASME: J. Fluids Engng* **115**, 436–443.

WILLIAMS, D. R., MANSY, H. & AMATO, C. 1992 The response and symmetry properties of a cylinder wake subjected to localized surface excitation. *J. Fluid Mech.* **234**, 71–96.

WILLIAMS-STUBER, K. & GHARIB, M. 1990 Transition from order to chaos in the wake of an airfoil. *J. Fluid Mech.* **213**, 29–57.

WINTERS, K. H. 1987 A bifurcation study of laminar flow in a curved tube of rectangular cross-section. *J. Fluid Mech.* **180**, 343–369.

WYGNANSKI, I., CHAMPAGNE, F. & MARASLI, B. 1986 On the large-scale structures in two-dimensional, small-deficit, turbulent wakes. *J. Fluid Mech.* **168**, 31–71.

YU, X. & LIU, J. T. C. 1991 The secondary instability in Goertler flow. *Phys. Fluids* A **3**, 1845–1847.